2019 IEEE/RSJ International Conference on Intelligent Robots and Systems (IROS)
Macau, China, November 4-8, 2019

A Novel Small-scale Turtle-inspired Amphibious Spherical Robot

Huiming Xing, *Student Member IEEE*, Shuxiang Guo, *Senior Member, IEEE*, Liwei Shi, Xihuan Hou, Yu Liu, Huikang Liu, Yao Hu, Debin Xia, Zan Li

***Abstract*—This paper describes a novel small-scale turtle-inspired Amphibious Spherical Robot (ASRobot) to accomplish exploration tasks in the restricted environment, such as amphibious areas and narrow underwater cave. A Legged, Multi-Vectored Water-Jet Composite Propulsion Mechanism (LMVWCPM) is designed with four legs, one of which contains three connecting rod parts, one water-jet thruster and three joints driven by digital servos. Using this mechanism, the robot is able to walk like amphibious turtles on various terrains and swim flexibly in submarine environment. A simplified kinematic model is established to analyze crawling gaits. With simulation of the crawling gait, the driving torques of different joints contributed to the choice of servos and the size of links of legs. Then we also modeled the robot in water and proposed several underwater locomotion. In order to assess the performance of the proposed robot, a series of experiments were carried out in the lab pool and on flat ground using the prototype robot. Experiments results verified the effectiveness of LMVWCPM and the amphibious control approaches.**

I. Introduction

Recently, much attention has been focused on autonomous amphibious robots. Owing to terrestrial and aquatic ability, amphibious robots are widely used in all kinds of high-risk tasks, such as monitoring and exploration, pollution detection, search and rescue, scientific investigation.

To achieve multiple locomotion modes in amphibious environment, such as snake-like, wheeled, legged, oscillatory, undulating and propellered, researches have proposed various robotic platforms using propulsive mechanisms. Different locomotion modes have strength and weaknesses. Legged robots cope better with uneven ground, but move slowly, while wheeled robots [1] walk rapidly but deal poorly with rough terrains; snake-like robots [2] move well on flat terrains but it is hard to adjust the direction and swimming velocity. In water, screws propellers-based robots are more stable and flexible than those with undulatory and oscillatory capacities. Therefore, many amphibious robots possess abilities of multiple locomotion modes.

Kim *et al.* proposed an amphibious robot prototype [3]. Using the buoyancy generated by spherical Styrofoam, it operates on water and walks on the ground. Zhang *et al.* built an amphibious robot named AmphiHex-I [4]. The robot is able to walk on rough terrain and maneuver in water. Besides, using the novel transformable flipper legs, the robot traverses terrain with soft muddy or sandy in amphibious areas. Using a novel variable stiffness legs combining the flexible flipper and the rigid fan-shaped leg structure, Zhong *et al.* developed an improved version- AmphiHex-II [5]. On-land and underwater locomotion performance of AmphiHex-II was improved highly. With an eccentric paddle mechanism based on the epicyclic gear mechanism, Shen *et al.* demonstrated an amphibious robot [6]. Using the rotational and oscillating paddling methods, this robot is able to perform various terrestrial and aquatic gaits.

Besides these normal amphibious robots, biology-inspired amphibious robotic has also been researched widely, such as snakes, fish, Natatores [7] and turtles. Guo *et al.* proposed a novel geometry mechanics-based serpentine gait for snake-like robots [8]. Crespi *et al.* developed a bio-inspired amphibious salamander robot [9]. With four legs and an active spine, the robot is able to swim in water and walk on ground with various gaits. Utilizing a wheel- propeller–fin mechanism and a specialized swivel mechanism, Yu *et al.* designed an amphibious biomimetic fish-like robot termed AmphiRobot-II [10]. The wheel–propeller–fin mechanism is regarded as a drive wheel for walking on land and as a common screw thruster or pectoral fin in water. Vogel *et al.* proposed RoboTerp, a quadrupedal amphibious robot [11] with a passive compliant mechanism in the lower leg. However, the robot cannot sink into the water but walk on land and swim on the water.

In this brief, a novel small-scale turtle-inspired amphibious spherical robot is proposed with a legged, multi-vectored water-jet composite propulsion mechanism. And the robot was able to walk like turtles on different terrains and swim flexibly in water. Legged locomotion can be used for the littoral environment. With multiple configurations of legs using LMVWCPM, ASRobot can realize hovering in water, floating and sinking, rotational locomotion with zero-radius. Compared with the previous amphibious robots [12-20], the robot was enhanced as follows: 1) The leg was designed with three joints driven by enhanced servomotors. The workspace of leg with three joints is larger than that with two joints. It is able to improve the flexibility, maneuverability and adaptability. 2) Improve the sensing abilities by carrying more sensors. 3) Using compact design and precision machining, improve the ability of waterproof and lose weight of the robot.

The rest of the paper is organized as follows. Section II presents the concept of the robot and introduces LMVWCPM. on-land model and gaits are given in Section III. The force analysis in water and multi-locomotion is elaborated in Section IV. Experimental results will be addressed in Section V. Finally, Section VI concludes the paper with an outline of future work.

* This work was supported by the National Natural Science Foundation of China (61503028, 61773064), Graduate Technological Innovation Project of Beijing Institute of Technology (2018CX10022) and National High Tech. Research and Development Program of China (No.2015AA043202).

Huiming Xing, Shuxiang Guo, Liwei Shi, Xihuan Hou, Yu Liu, Huikang Liu, Yao Hu, Debin Xia, Zan Li, are the Key Laboratory of Convergence Medical Engineering System and Healthcare Technology, the Ministry of Industry and Information Technology, Beijing Institute of Technology, No.5, Zhongguancun South Street, Haidian District, 100081 Beijing, China (corresponding authors to provide phones: +86-15911022732, +86-01068915908; e-mails: guo@eng.kagawa-u.ac.jp, shiliwei@bit.edu.cn).

Shuxiang Guo is also with the Faculty of Engineering, Kagawa University, 2217-20 Hayashi-cho, Takamatsu, Japan (e-mail: guo@eng.kagawa-u.ac.jp).

II. Design of The Amphibious Spherical Robot

A. Overall Mechanism

In consideration of the benefits of spherical robots, such as the stability of mechanical structure, the anti-disturbance performance, the sample kinematics model with three-plane symmetry, and the strong loading capacity, the amphibious spherical robot is built to monitor the littoral environment. As depicted in Figure 1, the robot mainly consists of a sealed cabin, a top shell that keeps stereo camera, Inertial Measurement Unit (IMU), a multiple pressure sensors-based artificial lateral line, the communication module, two quarter-spherical hulls, a central plate, LMVWCPM, and a detachable battery cabin with three batteries. Both the sealed cabin and the shell can keep a hemisphere shape. And with two quarter-spherical hulls, the robot keeps a spherical shape. A waterproof plug is mounted on the sealed cabin, and it connects the robot to remote computer via an optical fiber cable, which will assist in debugging the software easily. An O-ring is utilized between the seal cabin and the central plant to confirm waterproofing. In water, the robot swims like a ball with the two quarter-spherical hulls closed up. On land, the robot walks with two hulls opened.

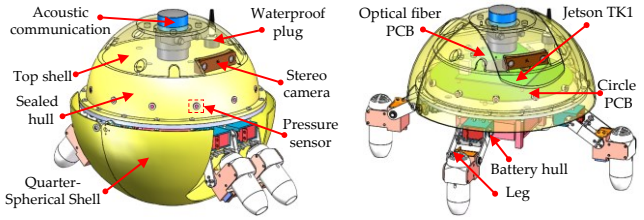

Figure 1. The structure of ASRobot. (a) Underwater configuration; (b) on-land configuration.

Assuring that the amphibious robot swims in water with the balance of gravity and buoyancy and walks on land flexibly, the most challenge is the rational design of the robot's weight and volume. The robot cannot walk with the heavier body smoothly, and if the gravity is larger than the buoyancy or less than the buoyancy, the robot will sink to the seabed or float to the water surface. If the robot requires an extra thrust to maintain hovering in water, it will cause an unnecessary energy consumption. Considering these aspects, the robot is designed using SolidWorks 2017 with powerful functions. One function is that the weight of one mechanical part can be calculated by selecting the texture. Finally, the volume of water discharged from the robot was approximately equal to the actual weight of the robot. And the weight of the robot is about 6.6Kg.

B. The Legged, Multi-Vectored Water-jet Composite Propulsion Mechanism

The proposed robot relied on LMVWCPM for on-land and underwater locomotion. As shown in Figure 2 (a), the composite driving mechanism has the radially free distributed structure. This structure is more superiorities than the traditional ones. The four cambered slides can keep four mechanical legs swinging smoothly. As shown in Figure 2 (b), the mechanical leg with 3 Degrees of Freedom (DoF) is composed of three digital servos, three connecting rod parts, one duct-type water-jet electric propeller and two bearings which make the leg rotate between the cambered slide and the middle plate steadily and smoothly. Three connecting rod parts are termed as coxa, femur and tibia respectively. And parameters of three connecting rod parts are shown in Table I. The joints linking these parts are named as follows: the joint linking the body and coxa is Thoraco-Coxal joint (TC-joint), and it keeps leg's forward and backward movements; the joint linking the coxa and femur is Coxa-Trochanteral joint (CTr-joint), which actuates elevation and depression of the leg; the joint linking the femur and tibia is Femur-Tibia joint (FTi-joint), which drives extension and flexion of the tibia. Three joints all are active joints actuated by servos named as Coxa Servo (CS), Femur Servo (FS) and Tibia Servo (TS), respectively. Thus, this composite driving mechanism enables the robot to crawl more flexibly on land and swim more swiftly in water.

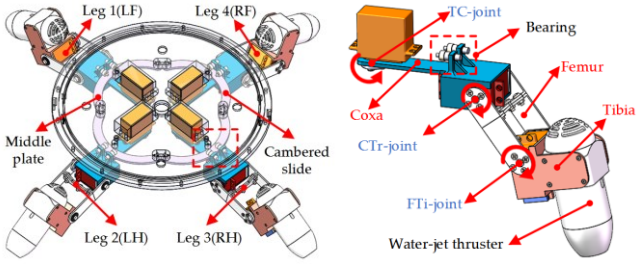

Figure 2. (a) The LMVWCPM; (b) One mechanical leg

III. On-Land Model

A. Forward and Inverse Kinematic Model on Land

To describe the locomotion of the robot simply, four legs are termed as LF, LH, RH, and RF [17]. As shown in Figure 3 (a), the coordinate system $\{O_B\}$ lied in the geometrical center of the body. The X_B, Y_B and Z_B axes represent the forward direction, the vertical direction (perpendicular to the body's horizontal plane) and the direction to the right of the body. The coordinate system $\{O_0^i\}$ represents the mobile base coordinate of the leg, and parameter i is leg index (1 for LF, 2 for LH, 3 for RH, and 4 for RF). As shown in Figure 3 (b), the coordinates $\{O_1^1\}$, $\{O_2^1\}$, $\{O_3^1\}$ and $\{O_4^1\}$ are built in TC-joint, CTr-joint, FTi-joint and the toe of LF.

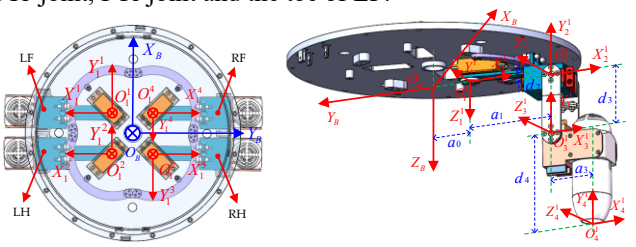

Figure 3. (a) The coordinates of ASRobot and legs(top view); (b) the coordinates of LF

TABLE I. The Denavit-Hartenberg (D-H) Parameters of LF

Joint j	θ_j^i	α_{j-1}^i	a_{j-1}^i	d_j^i	θ_j^i
1	$\theta_1^1(0)$	0	a_0	$d_1(0)$	$(0,\pi/2)$
2	$\theta_2^1(0)$	$-\pi/2$	$a_1(97)$	$d_2(10)$	$(-\pi/4,\pi/3)$
3	$\theta_3^1(0)$	0	0	$d_3(60)$	$(-\pi/6,\pi/2)$
4	0	0	$a_3(33)$	$d_4(85)$	0

Table I lists the Denavit-Hartenberg (D-H) parameters of LF. θ_j^i and d_j^i are the joint angle and the distance between the joint j-1 and j of leg i; α_{j-1}^i and a_{j-1}^i are the torsional angle and the length of the bar j-1 of leg i, respectively.

Using the D-H homogeneous transformation formula in the driven-axis context, the position of the LF toe in the mobile base coordinates is given by:

$$\mathbf{p}^1 = \begin{bmatrix} p_x^1 \\ p_y^1 \\ p_z^1 \end{bmatrix} = \begin{bmatrix} c_1^1 c_{23}^1 a_3 + c_1^1 s_{23}^1 d_4 + c_1^1 s_2^1 d_3 + c_1^1 a_1 \\ s_1^1 c_{23}^1 a_3 + s_1^1 s_{23}^1 d_4 + s_1^1 s_2^1 d_3 + s_1^1 a_1 \\ -s_{23}^1 a_3 + c_{23}^1 d_4 + c_2^1 d_3 + d_2 \end{bmatrix} \tag{1}$$

where, $a = \sqrt{2}/2$, $s_j^i = \sin\theta_j^i$, $c_j^i = \cos\theta_j^i$, $s_{jk}^i = \sin(\theta_j^i + \theta_k^i)$ and $c_{jk}^i = \cos(\theta_j^i + \theta_k^i)$, $(cs)_j^i = c_j^i - s_j^i$ ($i = 1,2,3,4$ and $j,k = 1,2,3$).

Similarly, equations of LH, RH and RF also is able to be acquired with the same procedure of LF.

In order to realize the robot movement, the inverse kinematic model needs to be built firstly. The inverse kinematic equations are derived via the forward kinematic model. Given that the toe position of LF is $\mathbf{p}_{\text{toe}}^1 = [p_x^1 \quad p_y^1 \quad p_z^1]^T$ in $\{O_0\}$, the position in other coordinate systems can be obtained by inverse transformation. The position in $\{O_1\}$ is given by Equation (2).

$${}^1T_4^1 = ({}^0T_1^1)^{-1}\,{}^0T_4^1 = {}^1T_2^1\,{}^2T_3^1\,{}^3T_4^1 \tag{2}$$

Then, Equation (3) containing two joint variables is obtained by Equation (2).

$$\begin{cases} -s_1^1 p_x^1 + c_1^1 p_y^1 = 0 \\ c_{23}^1 a_3 + s_{23}^1 d_4 + s_2^1 d_3 + a_1 = c_1^1 p_x^1 + s_1^1 p_y^1 \\ -s_{23}^1 a_3 + c_{23}^1 d_4 + c_2^1 d_3 + d_2 = p_z^1 \end{cases} \tag{3}$$

Define $m = c_1^1 p_x^1 + s_1^1 p_y^1 - a_1$, $t = (m^2 + n^2 - a_3^2 - d_4^2 - d_3^2)/2d_3$, and $n = p_z^1 - r_2$. θ_1^1 and θ_3^1 are obtained by Equation (4).

$$\begin{cases} \theta_1^1 = \operatorname{atan2}(p_y^1, p_x^1) \\ \theta_3^1 = \operatorname{atan2}(-a_3, d_4) - \operatorname{atan2}(t, \pm\sqrt{a_3^2 + d_4^2 - t^2}) \end{cases} \tag{4}$$

With this equation ${}^2T_4^1 = ({}^0T_1^1)^{-1}({}^1T_2^1)^{-1}\,{}^0T_4^1 = {}^2T_3^1\,{}^3T_4^1$, we can get Equation (5).

$$\begin{cases} c_1^1 c_2^1 p_x^1 + s_1^1 c_2^1 p_y^1 - s_2^1 p_z^1 + s_2^1 d_2 - c_2^1 a_1 = c_3^1 a_3 + s_3^1 d_4 \\ -c_1^1 s_2^1 p_x^1 - s_1^1 s_2^1 p_y^1 - c_2^1 p_z^1 + s_2^1 a_1 + c_2^1 d_2 = s_3^1 a_3 - c_3^1 d_4 - d_3 \end{cases} \tag{5}$$

Define $c_3^1 a_3 + s_3^1 d_4 = k$. The angle θ_2^1 is calculated by Equation (6).

$$\theta_2^1 = \operatorname{atan2}(m,n) - \operatorname{atan2}(k, \pm\sqrt{m^2 + n^2 - k^2}) \tag{6}$$

Similarly, equations of LH, RH and RF also can be acquired. where *IK* indicates the inverse kinematics, allowing mapping from the Cartesian space to the joint space.

B. Gaits

For quadruped robots with a lower body weight, many gaits, such as walking gaits, tripod gaits and trotting gaits, are designed mostly. However, ASRobot is much heavier than other quadruped robots to swim in water. It is a huge challenge to support the body with four legs and the leg needs to possess waterproofing. Therefore, only a crawling gait and a rotary gait were designed, which allowed the robot to walk like the turtle. The sequence of the crawling gait in one cycle is shown in Figure 4. The gray bar indicates the transfer phase, and the black and blue bars show the support phase. and moving body phase, respectively. Over single cycle of the crawling gait, the robot moves the body twice in support phase (blue bar) with four legs. Compared to the previous robot, ASRobot with three joints has plenty of advantages for flexibility, maneuverability and adaptability.

Figure 4. The sequence of the crawling gait and rotary gait.

Figure 4 also can describe the rotary gait. The most difference is the motion direction of the leg. If the legs all swing to the left, the robot will rotate to the left. The robot can rotate to the right with right swing of legs.

C. Simulation with ADAMS

To keep the robot crawl steadily and flexibly with its structural design, the choice of servomotors and the length of links is essential. A virtual simplified model of ASRobot is built and simulated in the ADAMS environment to measure the driving torques of different joints in the sit to stand motion and crawling motion.

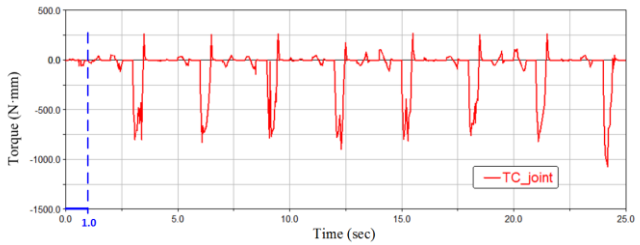

(a) the driving torque of TC-joint

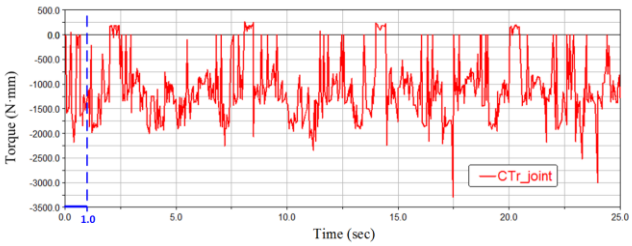

(b) the driving torque of CTr-joint

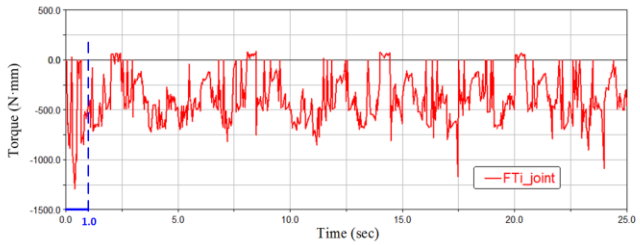

(c) the driving torque of FTi-joint

Figure 5. The driving torques of different joints in sit to stand motion and crawling with four cycles.

As shown in Figure 5, the sit to stand motion continues to 1s. From these curves, the driving torque of TC-joint is quite

small, and the driving torques of CTr-joint and FTi-joint are up to 2200 N • mm and 1300 N • mm. The crawling torque curves of different joints in LF is depicted from 1s to 25s (Figure 5), and conclusions are drawn as follows: First, the driving torques of CTr-joint and FTi are greater than that of the TC-joint; this is due to support the heavy body of ASRobot while crawling, and the TC-joint only swing the mechanical leg. The driving torque curves appear abrupt and form spikes, which will induce unbalanced moment and impact the stability of ASRobot. Second, for CTr-joint and FTi-joint, the driving torque in the support phase is much larger than the transfer phase. This is because four legs support the body in support phase and three legs support in transfer phase. Thirdly, during the support phase, the maximum driving torque of TC-joint basically remains steady and below 750 N • mm, and the maximum driving torques of CTr-joint and FTi-joint stay under 2250 N • mm and 1000 N • mm, respectively.

From simulation results of the sit to stand motion and crawling motion, CTr-joint requires the largest driving torque, about 22.5kg • cm. The driving torques of TC-joint and FTi-joint are below 10kg • cm. In the future, other heavy sensors will be installed in the robot, servomotors with larger toques in different joints are selected as shown in Table III and the length of leg components is shown in Table II.

TABLE II. LENGTH OF LEG COMPONENTS

Name	Coxa	Femur	Tibia
Length (mm)	99.43	62.00	32.75

TABLE III. SPECIFICATION OF SERVOMOTORS IN DIFFERENT JOINTS

Servomotors	CS	6.6V, 23 kg • cm, 0.12 s/60deg
	FS	8.4V, 38 kg • cm, 0.12 s/60deg
	TS	6.6V, 23 kg • cm, 0.12 s/60deg
Water-jet thruster		24V, 2A, 2.2N(Max)

IV. UNDERWATER MODEL

As shown in Figure 6, with symmetrical disposition of four legs, ASRobot has robust underwater motion under disturbances. The force analysis of the vectored propulsion is conducted in the horizontal and vertical propulsion.

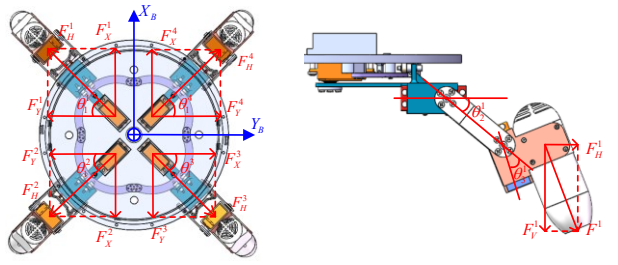

(a) (b)

Figure 6. The force analysis of LMVWCPM. (a) The force analysis of four propellers in horizontal plane; (b) the force analysis of one leg.

A. The Horizontal Propulsion Module

In the horizontal plane, the leg is driven by CS, and it can rotate around its axis within the bound $\theta_1^i \in [-\pi/4, \pi/4]$ (rad).

The thrust along the X axis:

$$F_X = -F^1 s_1^1 c_{23}^1 + F^2 s_1^2 c_{23}^2 + F^3 s_1^3 c_{23}^3 - F^4 s_1^4 c_{23}^4 \quad (7)$$

The thrust along the Y axis:

$$F_Y = -F^1 c_1^1 c_{23}^1 + F^2 c_1^2 c_{23}^2 + F^3 c_1^3 c_{23}^3 - F^4 c_1^4 c_{23}^4 \quad (8)$$

The moment on the Z axis:

$$T_Z = al[F^1 (cs)_1^1 c_{23}^1 + F^2 (cs)_1^2 c_{23}^2 + F^3 (cs)_1^3 c_{23}^3 + F^4 (cs)_1^4 c_{23}^4] \quad (9)$$

where, $a = \sqrt{2}/2$, $s_j^i = \sin\theta_j^i$, $c_j^i = \cos\theta_j^i$, $s_{jk}^i = \sin(\theta_j^i + \theta_k^i)$ and $c_{jk}^i = \cos(\theta_j^i + \theta_k^i)$, $(cs)_j^i = c_j^i - s_j^i$ ($i = 1,2,3,4$ and $j,k = 1,2,3$), l is the distance between the CS axis and the center of ASRobot.

B. The Vertical Propulsion Module

The vertical forces in Z axis direction of ASRobot is shown in Figure 6.

The thrust on the Z axis:

$$F_Z = F^1 s_{23}^1 + F^2 s_{23}^2 + F^3 s_{23}^3 + F^4 s_{23}^4 \quad (10)$$

The moment on the X axis:

$$T_X = al(-F^1 s_{23}^1 - F^2 s_{23}^2 + F^3 s_{23}^3 + F^4 s_{23}^4) \quad (11)$$

The moment on the Y axis:

$$T_Y = al(-F^1 s_{23}^1 + F^2 s_{23}^2 + F^3 s_{23}^3 - F^4 s_{23}^4) \quad (12)$$

Therefore, the force matrix $\mathbf{F}_B = [F_X \quad F_Y \quad F_Z]^T$ can be calculated by Equation (13).

$$\mathbf{F}_B = \mathbf{M}_F \mathbf{F}_P \quad (13)$$

where, the force vector $\mathbf{F}_P = [F^1 \quad F^2 \quad F^3 \quad F^4]^T$ of propellers, and the transformation matrix

$$\mathbf{M}_F = \begin{bmatrix} -s_1^1 c_{23}^1 & s_1^2 c_{23}^2 & s_1^3 c_{23}^3 & -s_1^4 c_{23}^4 \\ c_1^1 c_{23}^1 & c_1^2 c_{23}^2 & -c_1^3 c_{23}^3 & -c_1^4 c_{23}^4 \\ s_{23}^1 & s_{23}^2 & s_{23}^3 & s_{23}^4 \end{bmatrix} \quad (14)$$

And, the moment matrix $\mathbf{T}_B = [T_X \quad T_Y \quad T_Z]^T$ can be obtained by Equation (15).

$$\mathbf{T}_B = al\mathbf{M}_T \mathbf{F}_P \quad (15)$$

where,

$$\mathbf{M}_T = \begin{bmatrix} -s_{23}^1 & -s_{23}^2 & s_{23}^3 & s_{23}^4 \\ -s_{23}^1 & s_{23}^2 & s_{23}^3 & -s_{23}^4 \\ (cs_1^1)c_{23}^1 & (cs_1^2)c_{23}^2 & (cs_1^3)c_{23}^3 & (cs_1^4)c_{23}^4 \end{bmatrix} \quad (16)$$

V. EXPERIMENTS

A. On-land Locomotion Experiments

Considering the constraints of the structure of the legs, such as the swing angle of joints and the length of links, the largest stride length is 12cm. With this stride length, the robot can crawl steadily. As we all know, the speed of the robot depends on the stride frequency and length. Allowing for the limited performance of servos, the cycle of the crawling gait was set as 2s, 2.5s, 3s, 3.5s and 4s. As shown in Figure 7 (a), experiments of each cycle were conducted on smooth flat terrain five times to reduce the impact of incidental events. By recording the time and the distance the robot crawled, the velocities of the robot were obtained as shown in Figure 7 (b). The maximum velocity is up to 5cm /s at the cycle of 2s.

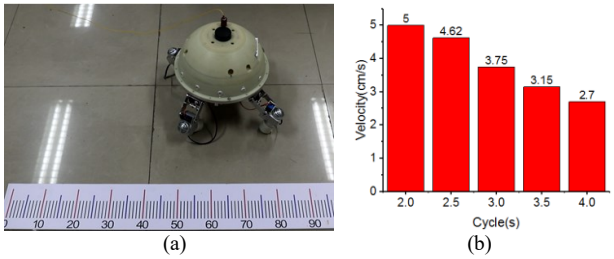

(a) (b)

Figure 7. Experiments of the crawling locomotion on smooth flat ground.

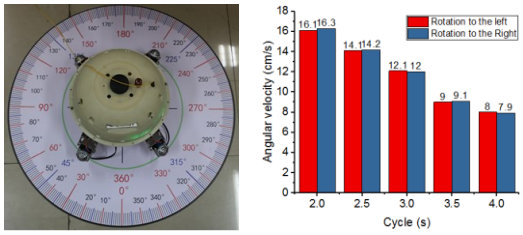

(a) (b)

Figure 8. Experiments of the rotating locomotion on smooth flat board.

Besides the crawling gait, experiments with the rotary gait were also conducted, i.e., rotation to the left and right. As shown in Figure 8 (a), a circle board with angle ruler is used to record the angle the robot rotates. The angular velocities of the rotation locomotion were obtained. As depicted in Figure 8 (b), at the cycle of 2s, the maximum angular velocities of rotation to the left and right are up to 16.1 deg/s and 16.3 deg/s, respectively. At this frequency, the robot can rotate steadily. As the frequency increases, an unstable phenomenon appears.

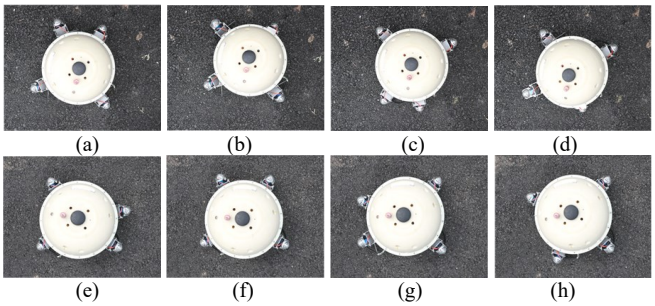

(a) (b) (c) (d)

(e) (f) (g) (h)

Figure 9. Snapshots of walking on asphalt ground. (a)-(d) The crawling gait; (e)-(h) the ratary gait.

(a) (b) (c) (d)

Figure 10. Snapshots of walking on different ground. (a) on grass land; (b) on sand grand; (c) on stone land; (d) on leaf ground.

Besides, crawling and rotating motion experiments on asphalt land were also conducted. As shown in Figure 9 (a)-(h), ASRobot crawls successfully on asphalt land. Due to greater friction on asphalt land, the maximum velocity of crawling is up to 5.3cm/s, and the maximum angular velocity is up to 16.8 deg/s. In order to prove the adaptability on different terrains, the robot was performed on grass land, sand land, stone land and leaf ground shown in Figure 10. The robot all walks flexibly and smoothly.

B. Underwater Locomotion Experiments

To evaluate underwater locomotion in the horizontal and vertical plane, several underwater experiments were conducted in the lab pool, the size of which is 3m×2m×1m (height×width×depth). In the pool, the water was static.

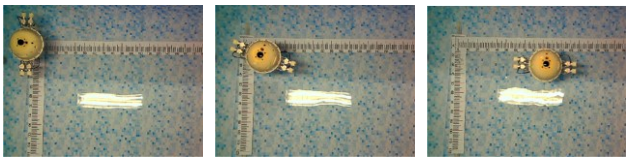

(a) (b) (c)

Figure 11. Snapshots of yaw control locomotion.

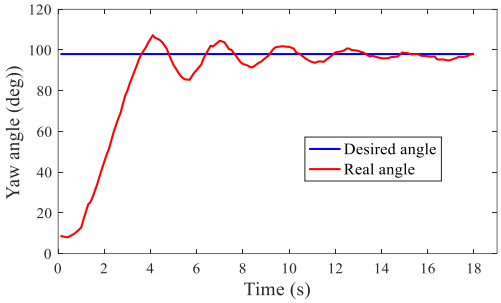

Figure 12. Experimental results of yaw control

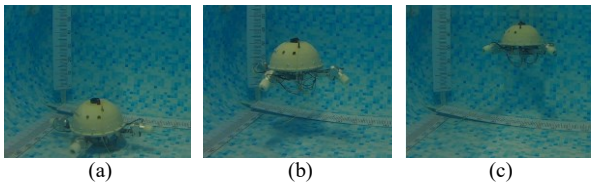

(a) (b) (c)

Figure 13. Snapshots of depth control locomotion.

With the previous work [16-22], yaw control experiment was conducted firstly. The yaw angle captured by JY901 IMU module is estimated using EKF. As shown in Figure 11, with the difference method of left water-jet thrust and right water-jet thrust, yaw control is realized. Figure 11 (a)-(c) shows snapshots from a video of yaw control. The initial angle is 8 deg, and the desired angle is 98 deg. From Figure 12, we can see that the robot can keep stable at 10s approximately and the mean error is up to 1.7 deg.

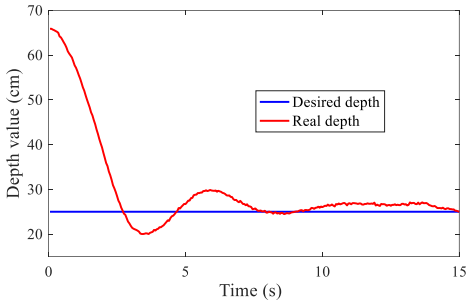

Figure 14. Experimental results of depth control locomotion

Depth control experiment was also conducted using a small-size pressure sensor (MS5803-01BA). The depth data is transported to the robot by IIC bus and served as the feedback for PID control. In this experiment, the initial depth of ASRobot is 65cm, and the desired depth is set to be 25cm. Figure 13(a)-(c) shows snapshots from a video of depth control. In Figure 14, the red curve illustrated the real depth. After 7.5s, the robot can achieve the desired depth and the mean depth error is 1.47cm.

Besides yaw control and depth control, the robot also is able to crawl on the bottom of river and sea. Because the equivalent gravity in water is less than that on land, the friction will decrease and the robot is easy to slip in water. Besides, the quicker the leg swing in water, the greater the drag on the robot. Therefore, the robot needs to adjust the frequency of the gait cycle. As shown in Figure 15 (a)-(h), ASRobot walked successfully on the bottom of the pool. The maximum velocity of crawling is up to 3.5cm/s at the cycle of 3s, and the maximum angular velocity is up to 11.5 deg/s.

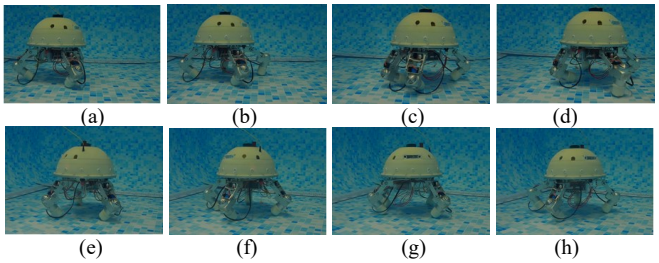

Figure 15. Snapshots of of underwater walking. (a)-(d) crawling gait; (e)-(h) rotary gait.

VI. Conclusion

This paper presents a novel small-scale turtle-inspired amphibious spherical robot which can accomplish exploration tasks in the restricted environment, such as amphibious areas and narrow underwater cave. A legged, multi-vectored water-jet composite propulsion mechanism was designed with four legs, one of which contains three connecting rod parts, three joints driven by digital servos and one water-jet thruster. Using a simplified kinematic mode and gaits design, the robot is able to crawl and rotate flexibly in different terrains. The maximum velocity and angular velocity are up to 5.3cm/s and 16.8 deg/s, respectively. On the bottom of the water pool, ASRobot can achieve the maximum crawling velocity of 4.5 cm/s and the maximum rotational velocity of 14.5 deg/s. Based on the analysis of the force and proposed locomotion in the submarine, yaw control and depth control experiments were conducted, and the robot can keep the desired angle with the mean error of 1.7 deg and the desired depth with the mean error of 1.47 cm. The performance of this robot is superior than the previous robots.

This study will give valuable references for design of small-sized amphibious robots. Transition motion between land and water will be studied.

References

[1] G. Freitas, F. Lizarralde, H. Liu, N. R. S. D. Reis, "Kinematic reconfigurability of mobile robots on irregular terrains," *IEEE International Conference on Robotics and Automation*, 2009, pp. 823-828.

[2] S. Hirose, H. Yamada, "Snake-like Robots: Machine Design of Biologically Inspired Robots," *IEEE Robotics & Automation Magazine*, vol. 16, no. 1, pp. 88-98, 2009.

[3] H. G. Kim, D. G. Lee, K. M. Jeong, T. W. Seo, "Water and Ground-Running Rootic Platform by Repeated Motion of Six Spherical Footpads," *IEEE/ASME Transactions on Mechatronics*, vol. 21, no. 1, pp. 175-183, 2016.

[4] S. Zhang, Y. Zhou, M. Xu, X. Liang, J. Liu, J. Yang, "AmphiHex-I: Locomotory Performance in Amphibious Environments with Specially Designed Transformable Flipper Legs," *IEEE/ASME Transactions on Mechatronics*, vol. 23, no. 2, pp. 1720-1731, 2018.

[5] B. Zhong, S. Zhang, M. Xu, Y. Zhou, T. Fang, W. Li, "On a CPG-based Hexapod Robot: AmphiHex-II with Variable Stiffness Legs," *IEEE/ASME Transactions on Mechatronics*, vol. 21, no. 3, pp. 542-551, 2016.

[6] Y. Shen, Y. Sun, H. Pu, S. Ma, "Experimental Verification of the Oscillating Paddling Gait for an ePaddle-EGM Amphibious Locomotion Mechanism," *IEEE Robotics & Automation Letters*, vol. 2, no. 4, pp. 2322-2327, 2017.

[7] H. Liu, L. Shi, S. Guo, H. Xing, X. Hou, Y. Liu, "Platform Design for a Natatores-like Amphibious robot," *IEEE International Conference on Mechatronics and Automation*, 2018, pp.1627-1632.

[8] X. Guo, S. Ma, B. Li, Y. Fang, "A Novel Serpentine Gait Generation Method for Snake-like Robots Based on Geometry Mechanics," *IEEE/ASME Transactions on Mechatronics*, vol. 23, no. 3, pp. 1249-1258, 2018.

[9] A. Crespi, K. Karakasiliotis, A. Guignard, A. J. Ijspeert, "Salamandra Robotica II: An Amphibious Robot to Study Salamander-Like Swimming and Walking Gaits," *IEEE Transactions on Robotics*, vol. 29, no. 2, pp. 308-320, 2013.

[10] J. Yu, R. Ding, Q. Yang, M. Tan, W. Wang, J. Zhang, "On a Bio-inspired Amphibious Robot Capable of Multimodal Motion," *IEEE/ASME Transactions on Mechatronics*, vol. 17, no. 5, pp. 847-856, 2012.

[11] A. R. Vogel, K. N. Kaipa, G. M. Krummel, H. A. Bruck, "Design of a compliance assisted quadrupedal amphibious robot," *IEEE International Conference on Robotics and Automation*, 2014, pp. 2378-2383.

[12] L. Shi, S. Guo, S. Mao, C. Yue, M. Li, K. Asaka, "Development of an amphibious turtle-inspired spherical mother robot," *Journal of Bionic Engineering*, vol. 10, no. 4, pp. 446-455, 2013.

[13] L. Shi, S. Pan, S. Guo, K. Tang, P. Guo, R. Xiao, Y, He, "Design and Evaluation of Quadruped Gaits for Amphibious Spherical Robots," *IEEE International Conference on Robotics and Biomimetics*, 2016, pp. 13-18.

[14] S. Guo, Y. He, L. Shi, S. Pan, R. Xiao, K. Tang, P. Guo, "Modeling and experimental evaluation of an improved amphibious robot with compact structure," *Robotics and Computer-Integrated Manufacturing*, vol. 51, pp. 37-52, 2018.

[15] H. Xing, S. Guo, L. Shi, Y. He, S. Su, Z. Chen, X. Hou, "Hybrid Locomotion Evaluation for a Novel Amphibious Spherical Robot," *Applied Sciences*, vol. 8, no. 2, pp. 156, 2018.

[16] X. Hou, S. Guo, L. Shi, H. Xing, S. Su, Z. Chen, Y. Liu, H. Liu, "Hydrodynamic Analysis of a Novel Thruster for Amphibious Sphere Robots," *IEEE International Conference on Mechatronics and Automation*, 2018, pp.1603-1608.

[17] S. Gu, S. Guo, "Performance Evaluation of a Novel Propulsion System for the Spherical Underwater Robot (SUR III)," *Applied Sciences*, vol. 7, no. 11, pp. 1196, 2017.

[18] H. Xing, L. Shi, K. Tang, S. Guo, X. Hou, Y. Liu, H. Liu, Y. Hu, "Robust RGB-D Camera and IMU Fusion-based Cooperative and Relative Close-range Localization for Multiple Turtle-inspired Amphibious Spherical Robots," *Journal of Bionic Engineering*, vol.16, no.3, pp.442-454, 2019.

[19] L. Zheng, S. Guo, S. Gu, "The communication and stability evaluation of amphibious spherical robots," *Microsystem Technologies*, vol.24, pp.1-12, 2018.

[20] H. Xing, S. Guo, L. Shi, X. Hou, Y. Liu, H. Liu, "Design, modeling and experimental evaluation of a legged, multi-vectored water-jet composite driving mechanism for an amphibious spherical robot," 10.1007/s00542-019-04536-7.

[21] H. Xing, S. Guo, L. Shi, S. Pan, Y. He, K. Tang, S. Su, Z. Chen, "Kalman Filter-based navigation system for the Amphibious Spherical Robot," *IEEE International Conference on Mechatronics and Automation*, 2017, pp. 638-643.

[22] H. Xing, S. Guo, L. Shi, X. Hou, S. Su, Z. Chen, Y. Liu, H. Liu, "Performance Evaluation of a Multi-Vectored Water-Jet Propellers Device for an Amphibious Spherical Robot," *IEEE International Conference on Mechatronics and Automation*, 2018, pp.1591-1596.